COMPUTER VISION AND IMAGE UNDERSTANDING
Vol. 72, No. 3, December, pp. 404–413, 1998
ARTICLE NO. IV980680

NOTE

Distance-Ordered Homotopic Thinning: A Skeletonization Algorithm for 3D Digital Images

Chris Pudney

Biomedical Confocal Microscopy Research Centre, Department of Pharmacology, The University of Western Australia, Nedlands, WA 6907, Australia
E-mail: cpudney@alphapharm.pharm.uwa.edu.au

Received February 3, 1997; accepted January 16, 1998

A technique called distance-ordered homotopic thinning (DOHT) for skeletonizing 3D binary images is presented. DOHT produces skeletons that are homotopic, thin, and medial. This is achieved by sequentially deleting points in ascending distance order until no more can be safely deleted. A point can be safely deleted only if doing so preserves topology. Distance information is provided by the chamfer distance transform, an integer approximation to the Euclidean distance transform. Two variations of DOHT are presented that arise from using different rules for preserving points. The first uses explicit rules for preserving the ends of medial axes or edges of medial surfaces, and the second preserves the centers of maximal balls identified from the chamfer distance transform. By thresholding the centers according to their distance values, the user can control the scale of features represented in the skeleton. Results are presented for real and synthetic 2D and 3D data. © 1998 Academic Press

1. INTRODUCTION

This paper presents a new algorithm for determining the skeleton of a three-dimensional (3D) binary image. Skeletons have been used to describe two-dimensional (2D) shapes since the 1960s [6, 8, 21] and are used in a variety of tasks in computer vision, such as pattern recognition, image segmentation, and image compression. Figure 1 shows a 2D example of a skeleton generated by the algorithm presented in this paper. The skeleton consists of a set of interconnecting curves (axes) within each foreground object. In 3D two types of skeleton are possible: the medial axes, composed of curves, as in the 2D case, or the medial surfaces composed of curves and surfaces. Figure 2 shows 3D examples of the medial axes and surfaces generated by the algorithm presented in this paper.

There is no precise definition of the skeleton of a digital image. Blum [6] used a grassfire analogy. The skeleton was defined as the locus of points at which the advancing firefront extinguished itself. Calabi and Harnett [8] defined the skeleton to be the set of centers of the maximal balls. A ball is centered on a foreground point and has radius equal to the distance from the point to the background of the image. Maximal balls are those that are not contained in any other ball. The definition used in this paper is as follows: a skeleton is a subset of the foreground objects that has the following properties:

Homotopy: The skeleton is topologically equivalent to the original image; that is, it has the same numbers of foreground objects, background objects and holes as the original image.

Thinness: The skeleton is one point wide.

Medialness: The skeleton is centrally located within the foreground objects.

These properties are listed in order of priority, that is, a skeleton is always thin except at points where a thick skeleton is necessary to satisfy homotopy. This can occur at some junctions in a skeleton. Similarly, a skeleton should be medial except at points where a noncentral skeleton is required to preserve topology or thinness. For example, where the foreground object has even width, a medial skeleton would have to be two points wide.

Most existing 3D skeletonization algorithms satisfy some but not all these properties. The algorithm presented in this paper is called *distance-ordered homotopic thinning* (DOHT) and produces skeletons that satisfy all three properties. It thins the foreground objects while preserving topology resulting in thin, homotopic skeletons. An important difference between DOHT and most other homotopic thinning techniques is that image points are processed in ascending distance order resulting in medial skeletons [29]. Distance information is provided by the distance transform, which can be computed beforehand [7, 9, 27] or on-the-fly [25]. Two variations of DOHT are presented: the first uses explicit rules for preserving either the ends of curves or the edges of surfaces during thinning. Techniques such as this are sensitive to noise and discretization of the image. A more robust version of DOHT is also presented that identifies the centers of maximal balls from the distance transform and preserves (a subset of) these during thinning.

1077-3142/98 $25.00
Copyright © 1998 by Academic Press
All rights of reproduction in any form reserved.

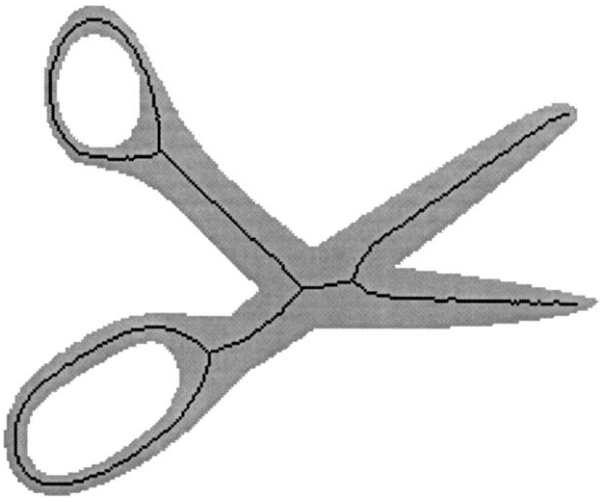

FIG. 1. A 2D binary image (gray foreground, white background) of a pair of scissors and its skeleton (black).

1.1. Definitions

Using the notation of Kong and Rosenfeld [15], a 3D binary image is defined as the quadruple $(\mathbb{Z}^3, m, n, F)$, where $\mathbb{Z}^3$ is the 3D cubic lattice on which the image points (voxels) are arranged, $(m, n) = (6, 26)$ or (26, 6), and $F \subseteq \mathbb{Z}^3$. A point $p \in \mathbb{Z}^3$ is defined by the triple (p_1, p_2, p_3) and has a value of 0 (*background*) or 1 (*foreground*). F is the set of foreground points, and m and n denote the foreground and background connectivities, respectively. Two foreground points are *neighbors* if they are m-adjacent, and two background points are neighbors if they are n-adjacent. Foreground points n-adjacent to the background are called *exterior* points; otherwise they are called *interior* points. The $3 \times 3 \times 3$ neighborhood of points centered on p is denoted by $N(p)$. Three subset neighborhoods are also defined: $N_6(p)$ denotes the set of points 6-adjacent to p, $N_{26}(p) = N(p) - \{p\}$ denotes the set of points 26-adjacent to p, and $N_{18}(p) = \{q \in N(p) : 1 \leq \sum_{i=1}^{3} |p_i - q_i| \leq 2\}$. Figure 3 shows these three neighborhoods.

1.2. Layout

The layout of this paper is as follows: Section 2 reviews existing techniques for skeletonizing 3D binary images and discusses topology preservation in 3D. The DOHT algorithm is presented in Section 3. This section describes an integer approximation to the Euclidean distance transform, rules for the deletion of points for medial axes and surfaces, and a version of DOHT that uses the centers of the maximal balls. Results are presented and discussed in Section 4, and the paper concludes with a discussion of future research in Section 5.

2. 3D SKELETONIZATION

The most popular approach for skeletonizing 3D binary images is *homotopic thinning* [12, 16, 17, 23, 29, 31, 32, 34]. Homotopic thinning successively deletes points from the foreground objects in such a way that the topology of the original image is preserved. Thinning stops when no more points can be safely deleted. This produces a homotopic, thin skeleton. However, the skeleton is not guaranteed to be medial.

The skeleton's position depends on the order in which points are deleted. Usually the order is arbitrary. Some researchers [17, 29, 31] iteratively delete individual points, while others [12, 16, 23, 32, 34] use parallel deletion, in which sets of multiple points are deleted simultaneously. Both techniques produce nonmedial skeletons. Saito's and Toriwaki's algorithm [29] does produce a medial skeleton. This is achieved by deleting points in ascending Euclidean distance order. They also show that this ordering results in stability of the skeleton under rotation. This idea forms the basis of the DOHT algorithm presented in this paper.

A common method for producing a medial skeleton in 2D is to identify points of symmetry from the distance transform of the image. The distance transform provides for each point the

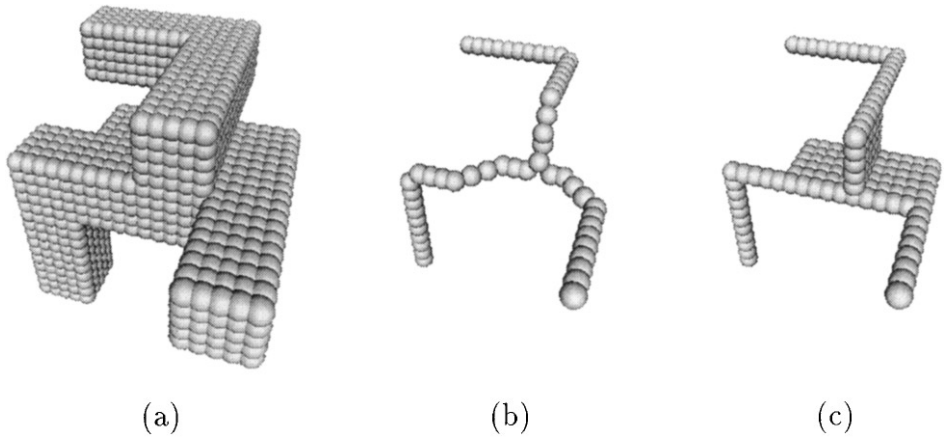

FIG. 2. (a) A 3D binary image, 3-L, and (b) its medial axes and (c) medial surfaces.

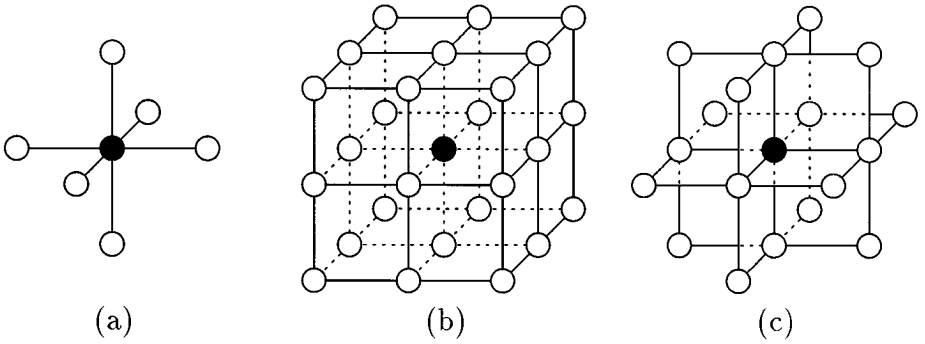

FIG. 3. The neighborhoods (open circles) (a) $N_6(p)$, (b) $N_{26}(p)$, and (c) $N_{18}(p)$ centered on a point p (closed circle).

shortest distance to a background point. A variety of distance metrics have been used, for example, the city block [28, p. 209], chessboard [1], and Euclidean [7, 9, 27] distances. Various types of points have been used as points of symmetry of the 2D distance transform: ridge points [1, 3], centers of maximal discs [4, 9, 11, 13, 22], conditional bisectors [30], and saddles and maxima [10, 33]. Malandain and Fernández-Vidal [19] successfully extended this approach to 3D images. They used hysteresis thresholding of the Euclidean distance transform to compute the medial surfaces of 3D images.

The symmetry points of the distance transform form a skeleton-like set of points that are centrally located within the foreground objects but, in general, are not topologically equivalent to the foreground objects and are not thin. Various techniques have been proposed to produce a topologically correct, thin skeleton from a set of 2D symmetry points. One approach is to trace ridges of the distance transform that run between disconnected symmetry points [3, 4, 10, 11, 22]. This produces a homotopic skeleton that is thin and medial. However, it is not obvious how to extend this method to 3D images. An alternative approach that extends to 3D is to homotopically thin the foreground objects while preserving the symmetry points [13, 30, 33]. However, the sections of skeleton connecting the symmetry points are not guaranteed to be medial because of the arbitrary order in which points can be deleted. In this paper, DOHT is used to connect the centers of maximal balls. This ensures that the final skeleton is medial. By pruning the set of centers of maximal balls before thinning, the influence of (discretization) noise on the skeleton can be controlled.

2.1. Topology Preservation

In homotopic thinning, points are deleted only if doing so preserves the topology of the image. Kong's and Rosenfeld's [15] definition of topology preservation requires that the output image be obtainable from the input image by sequential deletion of *simple* points. They provide the following theorem for determining whether a point is simple:

THEOREM 1. *Let p be a foreground point in a 3D binary image* $(\mathbb{Z}^3, m, n, F)$, *where* $(m, n) = (6, 26)$ *or* $(26, 6)$. *Let* $F' = F - \{p\}$. *Then p is a simple point if and only if the following conditions hold:*

1. p is m-adjacent to just one connected component of $N(p) \cap F'$.

2. p is n-adjacent to just one connected component of $N(p) - F$.

3. $\Delta\chi = \chi((\mathbb{Z}^3, m, n, N(p) \cap F)) - \chi((\mathbb{Z}^3, m, n, N(p) \cap F')) = 0$, *where* $\chi(B)$ *is the Euler characteristic of a 3D binary image B.*

Furthermore, conditions 1 and 3 together imply condition 2, and conditions 2 and 3 together imply condition 1 [15]. Note that these are local conditions; that is, they only depend on the arrangement of background and foreground points is $N(p)$.

Lobregt *et al.* [17] devised a fast method of checking the change in the Euler characteristic of a 3D binary image when a point p is deleted (condition 3). This is done by considering the contribution to $\chi(B)$ of the points in each of the octants of $N(p)$. The arrangement of background and foreground points in an octant can be encoded as an eight-bit word and used to index a lookup table containing Euler characteristic values.

Bertrand and Malandain [5] simplified the definition using two conditions that do not involve calculation of the Euler characteristic.

THEOREM 2. *Let p be a foreground point in a 3D binary image* $(\mathbb{Z}^3, m, n, F)$, *where* $(m, n) = (6, 26)$ *or* $(26, 6)$. *Let*

$$N^*(p) = \begin{cases} N_{18}(p) & \text{if } (m, n) = (6, 26) \\ N_{26}(p) & \text{if } (m, n) = (26, 6). \end{cases}$$

Then p is a simple point if and only if the following conditions hold:

1. p is m-adjacent to just one connected component of $N^*(p) \cap F$.

2. p is n-adjacent to just one connected component of $N^*(p) - F$.

3. DISTANCE-ORDERED HOMOTOPIC THINNING

The order in which points are deleted during homotopic thinning affects the position of the skeleton. This observation led to the development of the DOHT algorithm presented in this paper. As the name suggests it is a homotopic thinning technique with the important distinction that the order in which points are considered for deletion is determined by the distance transform; points are processed in *ascending distance order* resulting in a medial skeleton [29]. The skeleton is also homotopic because points are only deleted if doing so preserves topology, and the skeleton is thin because points are deleted until no more can be deleted.

Vincent [33] showed how homotopic thinning could be implemented efficiently by using queues. Pseudo-code inspired by Vincent's approach is presented in Fig. 4. To ensure points are processed in ascending distance order, a sorted queue is used. The initial loop places all exterior points on the queue. A label image tracks whether a point is queued. The main loop processes points from the head of the queue testing the deletability of each. Deletable points become background points and their foreground neighbors not already queued are placed on the sorted queue. This is done because deletion of a point affects the local topology and hence the deletability of its neighbors [15]. Deletability will be discussed in detail in Section 3.2. If a point is not deletable then it is labeled as such. The algorithm terminates when the queue is empty. At this stage no more points will be deletable. On termination, the image will have been skeletonized.

After the first pass of the main loop, the only points in the queue are those whose local topology has changed because of a deletion. This is efficient because only those points whose deletability must be assessed are processed. Many algorithms repeatedly scan the entire image to determine the exterior points and assess the deletability of them all regardless of whether their local neighborhoods have changed. The algorithm's complexity is $O(N + M)$, where N and M are the numbers of image points and nondeletable points that re-enter the queue, respectively. M depends on the topology of the image.

```
Input:  Binary image   Image[]     // Input image.
        Integer image  Distance[]  // Distance transform.
Output: Binary image   Image[]     // Skeletonised input image.

Q = NewSortedQueue();
for all image points p
  if (Exterior(p))
    Queue(Q, p, Distance[p])       // Queue exterior points in
    Label[p] = QUEUED              // ascending distance order.
  else
    Label[p] = UNQUEUED

while (!Empty(Q))                  // Process the queue until
  p = Head(Q)                      // empty.
  Label[p] = UNQUEUED
  if (Deletable(p))
    Image[p] = 0                   // Delete deletable points,
    for all n in N26(p)            // and queue their foreground
      if (Image[n] = 1 AND         // neighbours except those
        Label[n] != QUEUED)        // already queued.
        Queue(Q, n, Distance[n])
        Label[n] = QUEUED
  else
    Label[p] = NONDELETABLE        // Label non-deletable points.
```

FIG. 4. Pseudo-code for DOHT.

3.1. The Distance Transform

The DOHT algorithm uses the distance value of each foreground point. This can be provided by a distance transform, which can be computed beforehand or on-the-fly [25]. To ensure that a medial skeleton is produced the Euclidean distance transform should be used [9, 27]. In this paper an integer approximation to the Euclidean distance transform called the *chamfer distance transform* [7] is used. The chamfer distance is used rather than the exact Euclidean distance because it allows easy identification of the centers of maximal balls (see Section 3.2.2). Methods have been proposed for determining the centers of maximal discs from the exact Euclidean distance transform of a 2D image [4, 9, 11, 13]. However, 3D implementations of these methods are more expensive than using the chamfer distance.

The chamfer distance transform of a 3D binary image $(\mathbb{Z}^3, m, n, F)$ is defined recursively as follows:

$$d(p) = \begin{cases} \min\limits_{q \in N_{26}(p)} \{d(q) + D(p,q)\}, & p \in F \\ 0, & p \in \bar{F} \end{cases}, \qquad (1)$$

where $D(p, q)$ is an integer approximation to the Euclidean distance between pairs of adjacent points

$$D(p,q) = \begin{cases} n_1, & \|p-q\|^2 = 1 \\ n_2, & \|p-q\|^2 = 2 \\ n_3, & \|p-q\|^2 = 3 \end{cases}, \qquad (2)$$

where $n_i \in \mathbb{Z}$. Borgefors [7] showed that setting $n_1 = 3$, $n_2 = 4$, and $n_3 = 5$ minimized the upper bound on the difference between the chamfer and Euclidean distances. These are the values used in this paper. When these values are used the upper bound is $0.118r$, where r is the maximum radius of the object.

3.2. Deletability

An important component of DOHT is determining whether a point is deletable. Section 1.1 discussed the deletion of simple points such that topology is preserved. This section presents additional deletability constraints that produce medial axes or surfaces, provide noise tolerance, and delete points in parallel. Two variations of the DOHT algorithm arise by using different deletability rules:

Rule A. A point is deletable if it is simple and not the end of a medial axis or edge of a medial surface (see Section 3.2.1).

Rule B. A point is deletable if it is simple and not the center of a maximal ball with distance value greater than a user-defined threshold (see Section 3.2.2).

Rule A can produce skeletons that are sensitive to irregularities on the exterior of the foreground objects. A more robust result is obtained using Rule B. However, the latter can produce thick skeletons, so a two-stage DOHT algorithm is proposed: the first stage uses Rule B. The resulting thick skeleton is then thinned in the second stage by applying DOHT with Rule A.

3.2.1. Medial axis ends and medial surface edges. The medial axes are a set of interconnected curves. The ends of open curves are simple points, so they can be deleted without affecting the image's topology. Therefore an open curve can be reduced to a single point while preserving topology. Unfortunately, this does not maintain the shape characteristics of the original image. Thus the ends of open curves must be prevented from being deleted. To achieve this, end-points are identified as foreground points that have less than two foreground neighbors, so when determining the medial axes, a point is deletable if it is a simple point and not an end-point. The medial axes computed using this rule for the 3-L image are shown in Fig. 5(a).

A similar problem occurs when computing the medial surfaces because the edges of open surfaces are simple points. Several rules have been proposed to identify the edges of surfaces. For a point with coordinates (i, j, k), Tsao and Fu [32] used three checking planes $x = i$, $y = j$, and $z = k$, and defined edge points as having less than two foreground neighbors on any of these planes. Saito and Toriwaki [29] defined edge points as points that are not part of a simplex, which is any set of four noncoplanar, foreground points occupying the same octant. Lee and Kashyap [16] used a similar rule. Gong and Bertrand [12] defined an edge point as a simple point p that does not satisfy the rule

$$c \geq 8 \vee (4 \leq c \leq 7 \wedge (\exists i \in \{1, \ldots, 8\} : c_i = 3)),$$

where c is the number of foreground points in $N(p)$ and the c_i, $i = 1, \ldots, 8$ are the numbers of foreground points in the octants of $N(p)$.

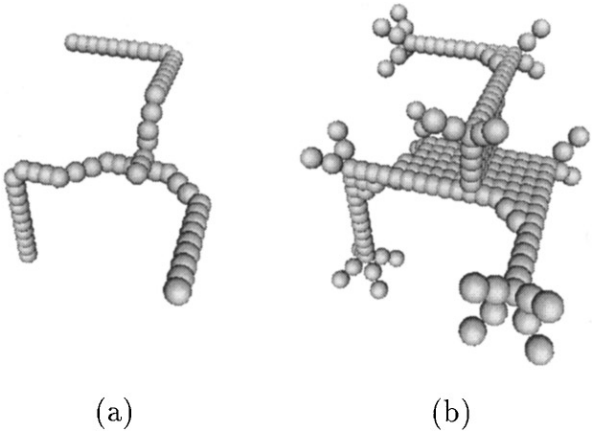

FIG. 5. (a) Medial axes and (b) medial surfaces of the 3-L image.

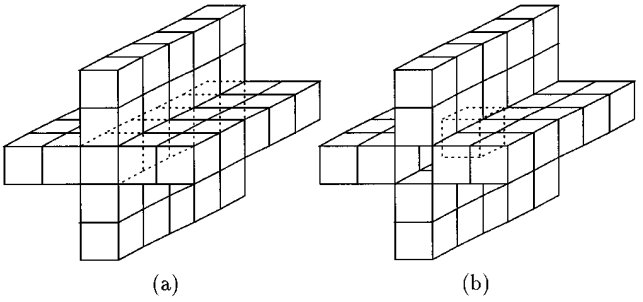

FIG. 6. (a) Edge points at the intersection of surfaces are not preserved by previous rules. This leads to (b) the reduction of surface intersections to a single point. Points on the intersection are shown with dashed lines.

None of these rules successfully identify edges at the intersection of multiple surfaces (see Fig. 6(a), for example). Using these rules results in the deletion of such edge points and the subsequent reduction of surface intersections to individual points, as in Fig. 6(b). A new rule has been developed that identifies surface edges including the edges of surface intersections.

At a point on the edge of a surface, a plane can be found that passes through the point such that the intersection of the plane and the surface includes an open curve that ends at the edge point. This is also true at surface intersections. For digital images, this observation is approximated by defining nine planes that pass through a point p and eight of its 26-neighbors. The planes are shown in Fig. 7. If p is the end of a curve on any of these planes, that is, if p has less than two foreground neighbors on any of the planes, then p is the edge of a surface. The medial surfaces computed using this rule for the 3-L image are shown in Fig. 5(b). As well as preserving the edges of surfaces, this rule also preserves sharp corners in the surface of the object. This results in axes in the skeleton that end at such corners. In Section 3.2.2 means of suppressing these axes are presented.

3.2.2. Centers of maximal balls. The rules presented in Section 3.2.1 for preserving the ends of curves and edges of surfaces are local in that they only examine the immediate neighborhood of the point under consideration. As such they can fail to distinguish between important global features to be preserved (ends of curves and edges of surfaces) and local features due to phenomena such as noise and discretization of the image. To overcome this problem, global rather than local features need to be preserved in the skeleton. One possibility is to preserve points of symmetry such as the centers of maximal balls.

Arcelli and Sanniti di Baja [2] showed that the centers of maximal disks can be identified from the chamfer distance transform of a 2D image. Their proof extends easily to 3D. The centers are the points p that satisfy

$$d(p) \neq d(q) - Dist(p, q), \forall q \in N_{26}(p), \tag{3}$$

where $d(p)$ and $D(p, q)$ are defined in Eqs. (1) and (2). Niblack *et al.* [22] called such points *nonwitness* points.

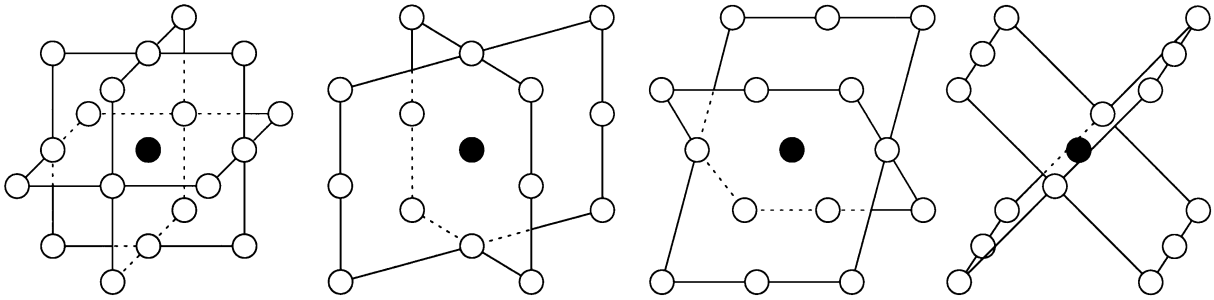

FIG. 7. The nine planes for checking the edge of a surface. The central point is the closed circle and its neighbors are the open circles.

Figures 8(a) and 8(b) show the nonwitness points of the 2D scissors image and 3D 3-L image, and Figs. 8(c) and 8(d) show the skeletons obtained by preserving these points during DOHT. For the 3-L image the nonwitness points and skeleton are identical. Note that each convexity in the 3D image induces a surface in the skeleton. This is precisely the effect that occurs when using the grassfire analogy to describe a skeleton [6].

Skeletons that include all the nonwitness points can be used to perfectly reconstruct the original image [22]. It was observed that the nonwitness points that reconstruct local variations on the exterior of the foreground objects are usually close to the exterior; that is, they have low distance values. This is particularly evident for the scissors image (see Fig. 8(a)).

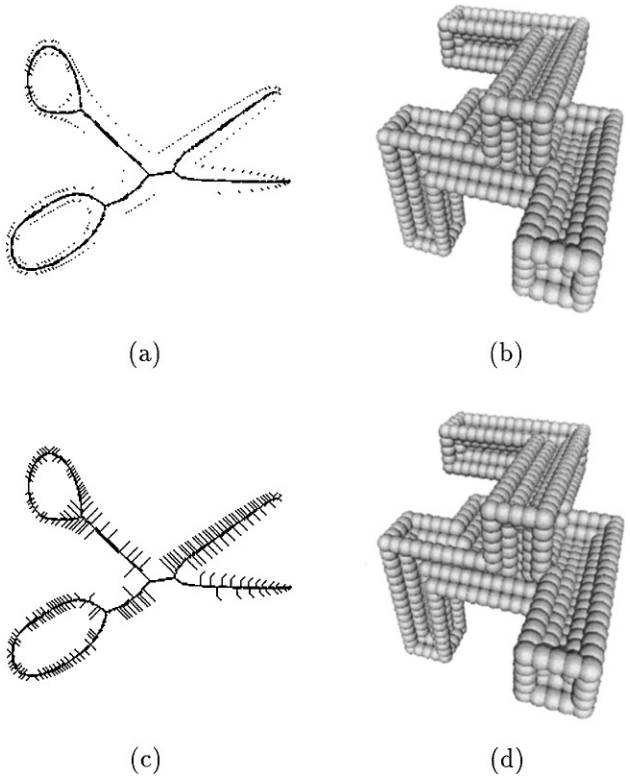

FIG. 8. The nonwitness points of the (a) scissors and (b) 3-L images, and the skeletons, (c) and (d), obtained by preserving these points during DOHT.

This observation led to the development of a two-stage DOHT algorithm in which the user can control the scale of features represented by the skeleton. The user defines a distance threshold τ, and then DOHT is performed such that nonwitness points with distance values greater than τ are preserved (Rule B). Preserving nonwitness points can produce a skeleton that is thick, so DOHT is applied to the output of the first stage this time preserving either the ends of curves or edges of surfaces, as in Section 3.2.1, depending on whether medial axes or surfaces are desired (Rule A). As τ increases the scale of features that are preserved in the skeleton also increases. In this way small scale features can be omitted from the skeleton. Fine structures that also have low distance values will also be omitted unless they are necessary for topology preservation.

The skeleton of the scissors image in Fig. 1 was produced using two-stage DOHT with $\tau = 6$. Recall that distance values are modulo $n_1 = 3$. Note that the noisy "spurs" present in Fig. 8(c) are suppressed. The medial axes and surfaces shown in Fig. 2 were also produced using two-stage DOHT with $\tau = 8$. Note for the medial surfaces that the axes induced by corners (see Fig. 5(b)) are suppressed as are the surfaces induced by convexities (see Fig. 8(d)).

Figure 9 shows a noisy version of the 3-L image. Noise has been added by randomly changing exterior foreground points to background points and randomly changing exterior background points (26-adjacent to foreground object) to foreground points. The figure also shows the medial axes and surfaces that result for $\tau = 7$. The essential shape characteristics of the original 3-L image are still present in these skeletons.

3.2.3. Parallel deletion. In the DOHT algorithms presented so far, points are deleted iteratively; that is, a point's deletability is assessed, if it is deletable then it is deleted, then the next point is processed, and so on. This can produce artifacts in the final skeleton. In practice, points are deleted in parallel; that is, a set of points is deleted simultaneously, then another set is deleted, and so on. Extra constraints must be satisfied to homotopically delete points in parallel [12, 14, 18, 23, 32, 34]. Recall that Theorems 1 and 2 require that points be deleted *sequentially* to preserve topology. For example, in Fig. 10 all points are simple, so if they are deleted simultaneously the object would disappear completely, breaking topology.

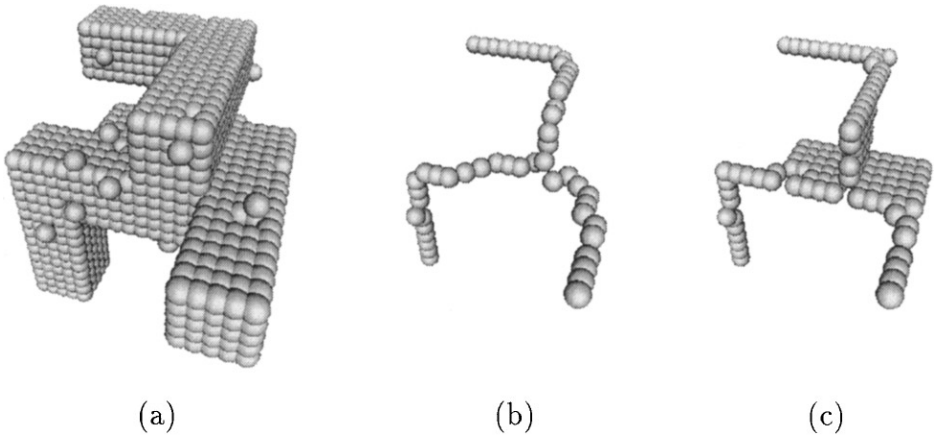

FIG. 9. The noisy 3-L image, and the medial axes and surfaces produced by two-stage DOHT with $\tau = 7$.

To avoid this problem a technique called *sequential rechecking* is used [16]. Sequential rechecking first determines all the deletable points without deleting any and then deletes them sequentially, rechecking their deletability before deletion. In DOHT, sequential rechecking is restricted to points with distance values equal to the current minimum distance.

4. RESULTS

Figure 11(a) shows a semi-transparent surface rendering of a $237 \times 191 \times 37$ magnetic resonance angiogram (MRA) and its medial axes. The image was segmented into foreground and background using expectation maximization and hysteresis thresholding [35]. The medial axes were computed using the two-stage DOHT described in Section 3.2.2. A threshold of $\tau = 3$ was used. Figure 11(b) shows a semi-transparent surface rendering of a $49 \times 43 \times 41$ confocal microscope image of a nerve terminal and its medial surfaces. The image was segmented into foreground and background by thresholding. The medial surfaces were computed using two-stage DOHT with a threshold of $\tau = 6$. Note that the medial surfaces are composed of axes and surfaces. Both images were resampled onto isotropic lattices, that is, lattices with equal spacing in the x-, y- and z-directions, before skeletonization. This introduces some smoothing but not enough to suppress noise.

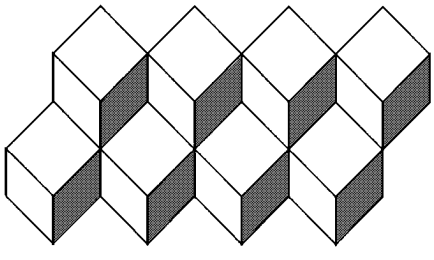

FIG. 10. All points are simple, deleting them simultaneously will break topology.

Table 1 summarizes the performance of the DOHT algorithm for the results presented in this paper. Processing times are from a DEC AlphaStation 250. More results for DOHT can be found in an earlier paper [25].

5. CONCLUSION

Distance-ordered homotopic thinning has been implemented and applied to a variety of real and synthetic 3D images. The resulting medial axes and surfaces show that DOHT is an effective and efficient technique for skeletonizing 3D images. By homotopically thinning points in ascending distance order a homotopic, thin, medial skeleton is produced. Rules for determining the medial axes or surfaces have been presented. The latter preserve important surface intersections. By thresholding the nonwitness points before skeletonization the scale of features represented by the skeleton can be controlled.

The current implementation of DOHT computes the medial axes directly from the image. It should also be possible to apply DOHT recursively such that the medial surfaces are computed and then DOHT is applied to the medial surfaces to produce the medial axes. The second stage would require a "geodesic" distance transform [24], that is, for each surface point, the shortest distance along the surface to the background (via a simple point such as the edge of a surface) is computed. This would produce medial axes that are centrally positioned within the medial surfaces.

Rather than using the chamfer distance transform an exact Euclidean distance transform can be used. Means of identifying the centers of maximal discs from the 2D Euclidean distance transform exist [4, 9, 11, 13]. These would need to be extended to 3D. The distance transform could also be modified to handle anisotropic images [20]. Such images have different spacing in the x-, y-, and z-directions and are common in biomedical imaging.

Although this paper has concentrated on 3D images, DOHT generalizes easily to any dimension; one need only provide the

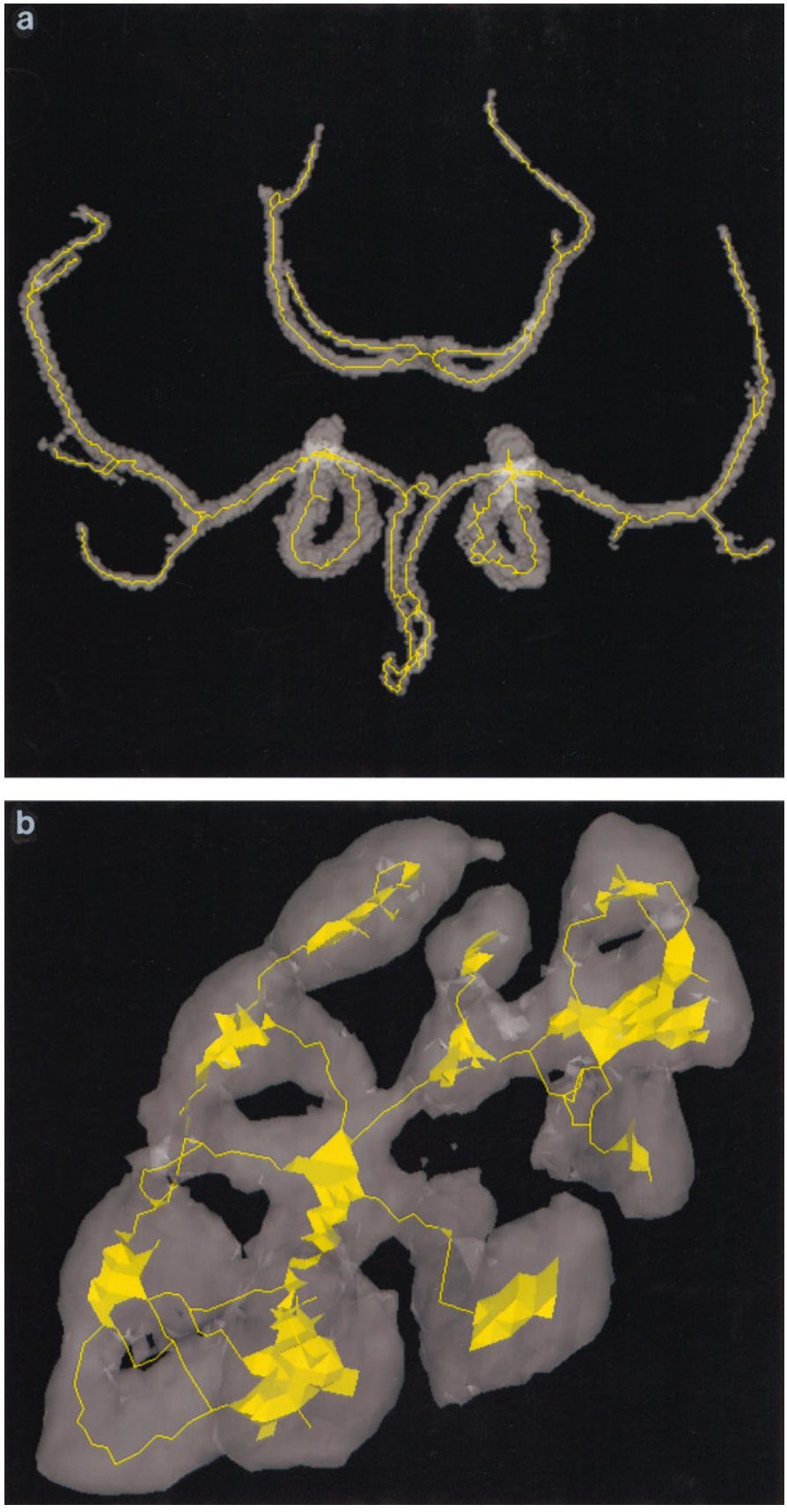

FIG. 11. (a) A magnetic resonance angiogram and the medial axes (yellow) computed using two-stage DOHT ($\tau = 4$). (b) A confocal microscope image of a nerve terminal, and the medial surfaces (yellow) computed using two-stage DOHT ($\tau = 6$).

TABLE 1
Performance Statistics for DOHT

Image (dimensions)	No. foreground points (original)	No. foreground points (skeleton)	Max. distance value	Processing time (*CPU s.*) Rule B	Processing time (*CPU s.*) Rule A	Processing time (*CPU s.*) Total
Scissors (256×256)	9997	600	54	0.3	0.07	0.37
3-L (axes) ($20 \times 27 \times 20$)	2050	54	11	0.14	0.017	0.16
3-L (surfaces) ($20 \times 27 \times 20$)	2050	134	11	0.14	0.017	0.16
MRA ($237 \times 191 \times 37$)	45866	1543	20	5.3	4	9.3
Confocal ($49 \times 43 \times 41$)	6678	580	12	0.46	0.1	0.56

rules for deletion of an n-dimensional point and the characterization of n-dimensional end-points. Some results for 2D images have been presented. DOHT algorithm can also be easily modified to skeletonize 3D gray-level images. This is achieved by supplying an integer-valued image as input to the basic DOHT algorithm. The algorithm homotopically thins the image in ascending gray-level order. This produces a tracing of the ridges of the input image. A version of this algorithm has been used as part of a feature detector that traces the ridges of the local energy map of 3D gray-level images [26].

ACKNOWLEDGMENTS

Many thanks to Michael Robins for his help with development of these techniques. The MRA data were provided by Dale Wilson and Dr. Alison Noble of the Department of Engineering Science, Oxford University, and Dr. James Byrne of the Neuroradiology Department, Radcliffe Infirmary, Oxford. The confocal microscope image was provided by Dr. Alan Everett of the Department of Physiology, The University of Western Australia. This research was supported by an R. W. Gibbon research fellowship and an A. Yeldham and M. Raine Research Foundation grant. The Biomedical Confocal Microscopy Research Centre gratefully acknowledges the support of the Lotteries Commission of Western Australia. I also thank my reviewers for their useful comments on the preparation of this paper.

REFERENCES

1. C. Arcelli and G. S. di Baja, A width independent fast thinning algorithm, *IEEE Trans. Pattern Anal. Mach. Intell.* **7**, 1985, 463–474.
2. C. Arcelli and G. Sanniti di Baja, Finding local maxima in a pseudo-Euclidean distance transform, *Comput. Vision Graphics Image Process.* **43**, 1988, 361–367.
3. C. Arcelli and G. Sanniti di Baja, Ridge points in Euclidean distance maps, *Pattern Recog. Lett.* **13**, 1992, 237–243.
4. C. Arcelli and G. Sanniti di Baja, Euclidean skeleton via centre-of-maximal-disc extraction, *Image Vision Comput.* **11**, 1993, 163–173.
5. G. Bertrand and G. Malandain, A new characterization of three-dimensional simple points, *Pattern Recog. Lett.* **2**, 1994, 169–175.
6. H. Blum, A transformation for extracting new descriptors of shape, in *Models for the Perception of Speech and Visual Form* (W. Wathen-Dunn, Ed.), pp. 362–380, MIT Press, Cambridge, MA, 1967.
7. G. Borgefors, Distance transformations in arbitrary dimensions, *Comput. Vision Graphics Image Process.* **27**, 1984, 321–345.
8. L. Calabi and W. E. Harnett, Shape recognition, prairie fires, convex deficiencies and skeletons, *Am. Math. Monthly* **75**, 1968, 335–342.
9. P. E. Danielsson, Euclidean distance mapping, *Comput. Graphics Image Process.* **14**, 1980, 227–248.
10. L. Dorst, Pseudo-Euclidean skeletons, in *Proceedings, 8th International Conference on Pattern Recognition, Paris, 1986,* pp. 286–288.
11. Y. Ge and J. M. Fitzpatrick, On the generation of skeletons from discrete Euclidean distance maps, *IEEE Trans. Pattern Anal. Mach. Intell.* **18**, 1996.
12. W. Gong and G. Bertrand, A simple parallel 3D thinning algorithm, in *Proceedings, International Conference on Pattern Recognition, Atlantic City, NJ, 1990*, IEEE Computer Society Press, pp. 188–190.
13. F. Klein and O. Kübler, Euclidean distance transformation and model guided image interpretation, *Pattern Recog. Lett.* **5**, 1987, 19–29.
14. T. Y. Kong, On the problem of determining whether a parallel reduction operator for n-dimensional binary images always preserves topology, in *Proceedings, Vision Geometry II*, SPIE, 1993, Vol. 2060, pp. 69–77.
15. T. Y. Kong and A. Rosenfeld, Digital topology: Introduction and survey, *Comput. Vision Graphics Image Process.* **46**, 1989, 357–393.
16. T.-C. Lee and R. L. Kashyap, Building skeleton models via 3-D medial surface/axis thinning algorithms, *CVGIP: Graphical Models Image Process.* **56**, 1994, 462–478.
17. S. Lobregt, P. W. Verbeek, and F. C. A. Groen, Three-dimensional skeletonization: Principle algorithm, *IEEE Trans. Pattern Anal. Mach. Intell.* **2**, 1980, 75–77.
18. C. M. Ma, On topology preservation in 3D thinning, *Image Understanding* **59**, 1994, 328–339.
19. G. Malandain and S. Fernández-Vidal, Topologically correct skeleton in n-d, in *Proceedings, 5th Discrete Geometry for Computer Imagery, Clermont-Ferrand, France, 1995*, pp. 199–208.
20. J. F. Mangin, I. Bloch, J. López-Krahe, and V. Frouin, Chamfer distances in anisotropic 3D images, in *Proceedings, VII European Signal Processing Conference, Edinburgh, 1994.*
21. U. Montanari, A method for obtaining skeletons using quasi-Euclidean distance, *J. Assoc. Comput. Mach.* **15**, 1968, 600–624.
22. C. W. Niblack, P. B. Gibbons, and D. W. Capson, Generating skeletons and center-lines from the distance transform, *CVGIP: Graphical Models and Image Processing* **54**, 1992, 420–437.
23. K. Palágyi and A. Kuba, A thinning algorithm to extract medial lines from 3D medical images, in *Proceedings, XVth International Conference on*

Information Processing in Medical Imaging (IPMI97), Poultney, VT, 1997, pp. 411–416.

24. J. Piper and E. Granum, Computing distance transformations in convex and nonconvex domains, *Pattern Recog.* **20**, 1987, 599–615.
25. C. J. Pudney, Distance-based skeletonization of 3D images, in *Proceedings, TENCON'96: IEEE Region 10 Conference on Digital Signal Processing Applications, Perth, WA, 1996*, pp. 209–214.
26. C. J. Pudney, M. J. Robins, B. J. Robbins, and P. D. Kovesi, Surface detection in 3D confocal microscope images via local energy and ridge tracing, *J. Comput. Assisted Microscopy* **8**, 1996, 5–20.
27. I. Ragnemalm, The Euclidean distance transform in arbitrary dimensions, *Pattern Recog. Lett.* **14**, 1993, 883–888.
28. A. Rosenfeld and A. C. Kak, *Digital Picture Processing*, 2nd ed., Vol. 2, Academic Press, New York, 1982.
29. T. Saito and J.-I. Toriwaki, A sequential thinning algorithm for three dimensional digital pictures using the Euclidean distance transformation, in *Proceedings, 9th Scandinavian Conference on Image Analysis (SCIA'95), Uppsala, Sweden, IAPR, 1995*, pp. 507–516.
30. H. Talbot and L. Vincent, Euclidean skeletons and conditional bisectors, in *Proceedings, Visual Communications and Image Processing, SPIE, 1992*, Vol. 1818, pp. 862–876.
31. J. Toriwaki and S. Yokoi, Algorithms for skeletonizing three-dimensional digitized binary images, in *Proceedings, Architecture and Algorithms for Digital Image Processing, SPIE, 1983*, Vol. 435, pp. 25–26.
32. Y. F. Tsao and K. S. Fu, A parallel thinning algorithm for 3D pictures, *Comput. Graphics Image Process.* **17**, 1981, 315–331.
33. L. Vincent, Efficient computation of various types of skeletons, in *Proceedings, Image Process., SPIE, 1991*, Vol. 1445, pp. 297–311.
34. R. Watzel, K. Braun, A. Hess, H. Scheich, and W. Zuschratter, On the deletability of points in 3D thinning, in *Proceedings, Image Analysis Applications and Computer Graphics: Third International Computer Science Conference, ICSC'95, Hong Kong, 1995*, pp. 91–98.
35. D. Wilson, A. Noble, and C. Pudney, From MR angiography to x-ray angiography, in *Proceedings, Medical Image Analysis and Understanding '97, Oxford, UK, 1997*, pp. 161–165.